Collapsed carbon nanotubes as building blocks for high-performance thermal materials

Jihong Al-Ghalith, Hao Xu, and Traian Dumitrică

Phys. Rev. Materials **1**, 056001 — Published 25 October 2017

DOI: 10.1103/PhysRevMaterials.1.056001

Collapsed Carbon Nanotubes as Building Blocks for High-Performance Thermal Materials

Jihong Al-Ghalith,[1] Hao Xu,[2] and Traian Dumitrică[1,2,]*

[1]Department of Mechanical Engineering, University of Minnesota, Twin Cities, MN 55455

[2]Department of Aerospace Engineering and Mechanics, University of Minnesota, Twin Cities, MN 55455

Corresponding Author *E-mail: dtraian@umn.edu

Abstract

The influence of collapsed shape on the thermal transport of carbon nanotubes is studied by non-equilibrium molecular dynamics. Nanotubes of different lengths, diameters, chiralities, and degrees of twist are simulated in the regime in which the thermal transport extends from ballistic to diffusive. In contrast with graphene nanoribbons, which are known to exhibit substantial rough-edge and cross-plain phonon scatterings, the collapsed tubes preserve the quasi-ballistic phononic transport encountered in cylindrical nanotubes. Stacked-collapsed nanotube architectures, closely related with the strain-induced aligned tubes occurring in stretched nanotube sheets, are shown to inherit the ultra-high thermal conductivities of individual tubes, and are therefore proposed to form highways for efficient heat transport in lightweight composite materials.

I. INTRODUCTION

The continuous advances in carbon nanotube (CNT) processing technology have brought about a new class of synthetic materials, which include large-volume CNT sheets suitable for developing macroscale applications [1]. The sheet exhibits a network structure comprising partially aligned and highly-entangled mm-long CNTs, which gives rise to a large variety of physical properties [2, 3]. Currently, there are significant efforts to manipulate CNT orientation [4] in order to control macro-scale properties and impart the network the exceptional mechanical, thermal and electrical attributes of individual CNTs [5, 6]. For example, by mechanically stretching CNT sheets [4], a 22-fold improvement in the Young's modulus and a 44% increase in electrical conductivity along the stretch direction have been reported [7]. Interestingly, recent atomic-resolution transmission electron microscopy analysis of the stretched-processed sheets [8] found massive presence of long, flattened CNTs [9]. Thus, during sheet stretching, the initially-cylindrical large-diameter CNTs undergo not only alignments but also permanent radial collapse to a dog-bone-shaped cross-section.

The thermal properties of CNTs are of significant interest since the thermal conductivity (κ) of suspended single-walled cylindrical CNTs – 1,500 - 3,500 W m^{-1} K^{-1} at room temperature [6, 10, 11] – is comparable with the in-plane κ of graphite and diamond, which are among the best known thermal conducting materials. Molecular dynamics (MD) simulations showed that defects in CNTs, including bends and kinks, could significantly reduce κ as they strongly suppress high-frequency phonon modes [12]. Although the existence of collapsed CNTs has been known for decades [13], and their energetic stability, mechanical and electronic properties are well understood [14-16], thermal transport along these nanostructures has received less

attention. The impact on κ of the CNT circumference collapse, in which opposite faces form a van der Waals (vdW) bi-layer with two nearly circular edges, Figure 1a, is not known. This is a valid problem, since edges [17, 18] and cross-layer scattering [19, 20] can drastically impact the heat carrying abilities of graphitic materials. Additionally, collapsed CNTs are very susceptible to torsional deformations [21, 16], which might also affect κ.

By way of non-equilibrium MD simulations carried out with LAMMPS [22], here we examine phononic transport, which is expected to be the dominant component of the thermal transport in both metallic and semiconducting CNTs [11]. We consider not only individual CNT structures, Figure 1a, but also tightly-packed collapsed CNT systems, Figure 1b, to probe the robustness of the thermal transport to the potential quenching of the heat-carrying phonon modes by neighboring CNTs. To this end, we investigated various morphologies, including isolated collapsed single-walled CNTs, and experimentally relevant [9] collapsed CNT stacks. To probe the edge, layer-coupling, width, chirality, twist and the number-of-tubes structural effects, as well as the CNTs length scales needed to cover both the ballistic and diffusive transport, we simulated systems containing up to 1,228,800 carbon atoms.

II. COMPUTATIONAL METHODS

To prepare the collapsed CNTs, a Nose-Hoover thermostat was used initially to equilibrate the cylindrical CNTs at 5K. After the system reached equilibrium, a 0.01eV/Angstrom force was added in the transverse direction for 15 ps to squeeze the structure. The system was then freed in the transverse direction and equilibrated again under microcanonical ensemble for another 500 ps. Periodic boundary conditions were applied in the axial direction throughout the whole process. In the end, we used conjugate gradient relaxation to relax the collapsed structures at 0K. The structures remained collapsed during the subsequent MD studies. The twisted collapsed

CNTs were created by performing structural relaxations under objective boundary conditions [23]. The packed collapsed CNTs were created via relaxations under triclinic periodic boundary

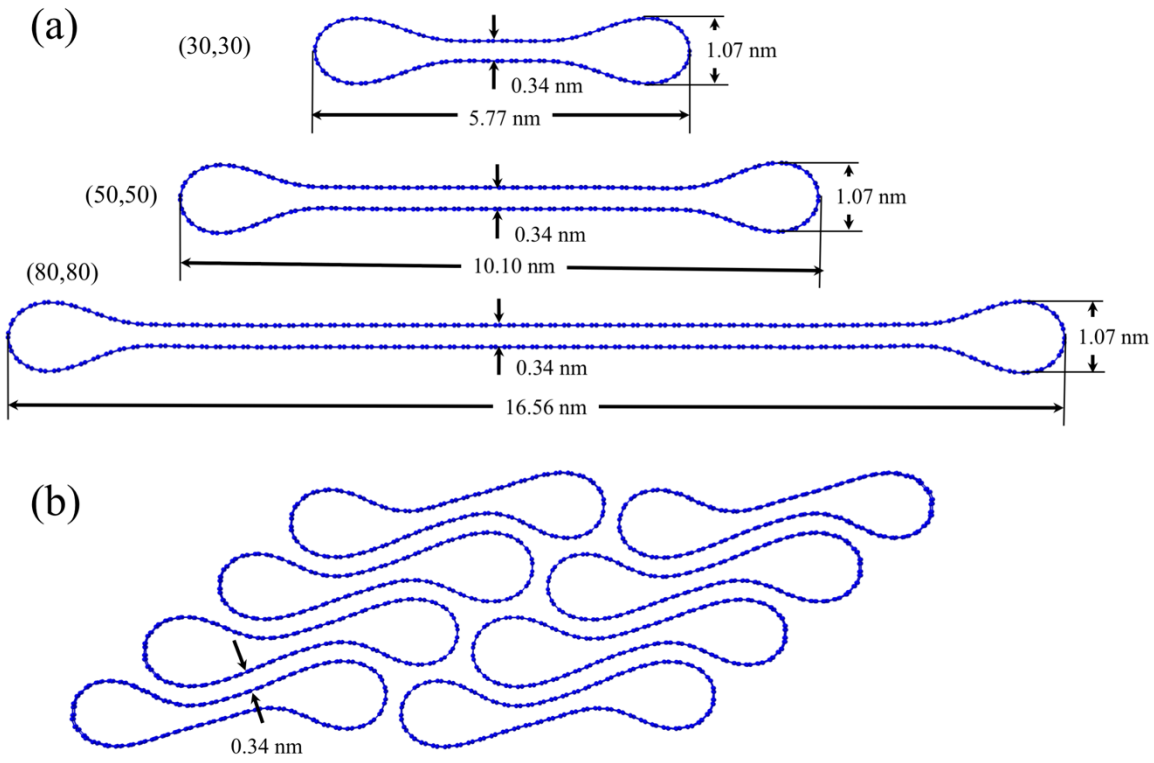

conditions.

Figure 1. Cross section of the optimized (a) collapsed (30,30), (50,50) and (80,80) CNTs (from top to bottom), and (b) stacked collapsed (30,30) CNTs.

Figure 2. Diameter (D) of the nearly-circular edges of (*n*, *n*) CNTs versus *n*, as calculated with several bond-order potentials. The force-field data is taken from Ref. [15].

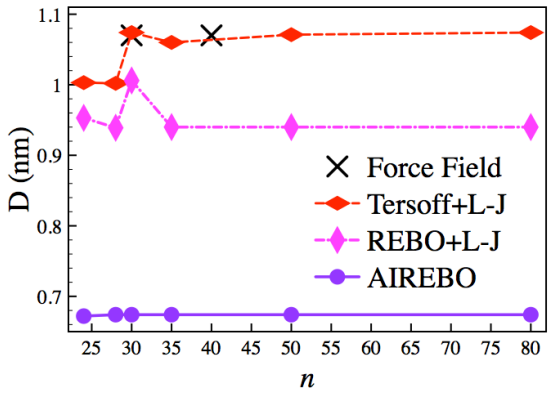

The geometry of the collapsed CNTs balances the bending energy stored in the bulging, nearly-circularizing edges with the vdW energy gained from drawing the flattened CNT walls close together. Thus, the interatomic forces play a dominant role in establishing the shapes of the collapsed CNTs. The selection of the interatomic classical potential is particularly subtle as the molecular mechanics of the available bond-order potentials with vdW interactions – AIREBO [24] and REBO [25] – describe bending strain differently [26]. In this respect, Figure 2 shows that the nearly-circular edges of the collapsed single-walled CNTs present different diameters, even when the same Lennard-Jones (L-J) parameters (energy parameter $\varepsilon = 2.84$ meV and the distance parameter $\sigma = 3.4$ Å) are used to describe the vdW interactions. We selected the Tersoff potential [27] for our calculations, which was optimized to produce a phonon dispersion for the heat carrying phonon modes of CNTs and graphene in good agreement with experimental evidence [28]. To describe the collapsed CNTs, we have further added L-J interactions between the C-C atoms located on opposite faces with L-J parameters ($\varepsilon = 3.5$ meV and $\sigma = 3.4$ Å) adjusted to describe stress-free collapsed geometries similar to those obtained with accurate force fields derived from *ab initio* calculations and experiments [14, 15].

The set-up used for the κ calculations is described in Figure 3a-b. One-unit cell ring at each end of the tube was kept fixed throughout the simulation to prevent the center of the mass of the system from moving, and to impose a torsional deformation. Four other neighboring unit cells were designated as "hot" and "cold" baths. In selecting a simulation set-up with relatively small bath regions, we have followed the guidelines of Salaway and Zhigilei [29], which emerged from systematic length-dependent convergence studies of κ performed in cylindrical CNTs. We have also adopted their notion that κ reflects not only the thermal behavior of the CNT portion located

between the bath regions, but also of the bath regions themselves. In this respect, our tests on large-diameter collapsed CNTs with different sizes of bath region produced stable thermal

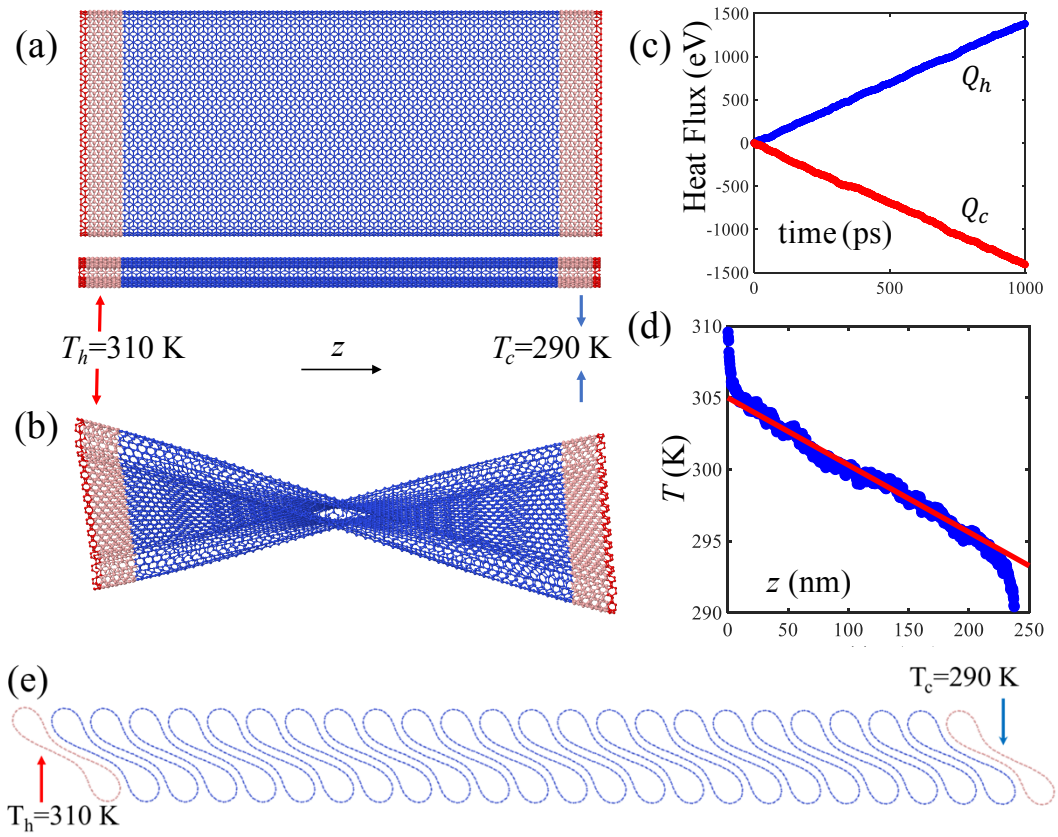

conductivities in different CNT length regimes, Figure S1 [30]. Therefore, in our subsequent κ *vs* length plots, we have used the CNT length with the bath regions included.

Figure 3. Non-equilibrium MD setup for (a) straight and (b) twisted collapsed (30,30) CNTs. The twist rate is 0.105 rad/nm. (c) Temperature (blue circles) profiles in a straight (30,30) CNTs 250 nm in length. The fitted line is shown in red. (d) The heat fluxes flowing into the hot Q_h and cold reservoir Q_c at the steady state. (e) Non-equilibrium MD setup for computing the inter-tube thermal resistance R in a stack of 23 collapsed (30,30) CNTs.

In preparation for the thermal calculations, the system was initially equilibrated at 300 K with a Nose-Hoover thermostat after which the two reservoirs were rescaled at every time step to

maintain $T_h = 310$ K and $T_c = 290$ K, respectively. Under velocity Verlet cycling with a 0.5 fs time step, a steady state was reached after 1,000 ps or longer, depending on the sample length. The collapsed CNT shape without any edge breaking was maintained throughout the MD simulation, Figure S2 [30]. The heat flux along CNTs was obtained by calculating the difference of the rate of the kinetic energy extraction from the two reservoirs $\dot{Q} = 0.5 < \dot{Q}_h - \dot{Q}_c >$, where $\dot{Q}_h$ and $\dot{Q}_c$ are the instantaneous heat currents flowing into and away from the hot and cold baths to maintain the temperature gradient, Figure 3c. The angular brackets indicate a statistical average taken after the steady state was reached. From the dependence of the local temperature T, obtained here by statistically averaging the kinetic energy of the atoms located in one unit cell, on the axial position z, we obtained the temperature profile shown in Figure 3d. To minimize the effects of fluctuations in local T, the κ presented in each figure is the average of five data sets taken after reaching the steady state. Accordingly, the error bars in each figure represent the standard deviation. κ is calculated with Fourier's law $\kappa = -\dot{q}(dT/dz)^{-1}$. Here $\dot{q}$ is $\dot{Q}$ per cross-sectional area, which is defined here by the thickness of the single atomic layer in a tube wall, 0.34 nm, multiplied by the circumference of the cylindrical CNT. For collapsed CNTs, the inextensible deformation approximation is justified in view of the large width of the bi-layer region and the nm-scale diameter of the nearly-circular edges [26]. Therefore, the cross-sectional area of collapsed CNTs is taken to be the same as that of the original cylindrical CNT. Any potential changes in κ under circumferential collapse reported next cannot be attributed to different definitions of the cross-sectional area.

For the calculations of the interfacial thermal resistance R between collapsed (30,30) CNTs, heat baths were applied on the left and right CNTs of the stack, as shown in Figure 3e. The CNTs between the two heat baths are free to move. R between tubes is calculated from $(N-1)\cdot$

$R = L/\kappa_i$, where κ_i is the computed thermal conductivity in the interfacial direction (y direction), L and N are the total between-bath distance and the number of CNTs between the two heat baths, respectively. The contact area is 18.7 nm^2, as approximated by the width of the collapsed CNT in vdW contact of 5 nm times the PBC length in the z direction.

III. RESULTS AND DISCUSSION

III. 1. Thermal Transport in Individual CNTs

Before discussing the impact of the collapsed shape, it is important to first review the behavior of thermal transport in cylindrical CNTs. It is known that CNTs exhibit strong ballistic behavior over submicron length scales [31-34]. Figures 4a and 4b show that the sample length l of both (30,30) and (50,0) CNTs strongly influences κ. The initial linear increase of $\kappa \propto l$ is a signature of pure ballistic behavior, i.e. phonons are able to propagate without being scattered by the sample. As the sample length increases, more phonon modes with longer wavelengths are being supported. These modes were shown to contribute actively to an increase of κ [32], although in a non-linear way. Another important feature is the significantly lower rate $\kappa \propto l^{0.2}$ of increase at sample lengths above ~200 nm, which signals that the thermal transport extends into the diffusive regime. κ shows signs of saturations at above ~600 nm and the slow increase exhibited beyond this length is expected to continue over micron length scales [31-34].

Figures 4a and 4b also show that the three considered inter-atomic potentials produce similar trends but very different κ magnitudes. To rationalize this result, we recall that the phonon dispersion plays an important role in thermal transport. While the re-optimized Tersoff potential [28] captures the quadratic behavior of the lowest frequency phonon modes near the Γ point, the REBO [25] and AIREBO [24] potentials produce linear behaviors in this region, Figure S2 [30]. This artifact causes significant error in κ, specifically a 50-80% underestimation

of κ by the REBO and AIREBO when compared to the re-optimized Tersoff potential result. It is worth noting that for the longest considered cylindrical CNTs, the κ produced by the re-optimized Tersoff potential of 1,600-2,000 $\mathrm{W\,m^{-1}\,K^{-1}}$, is consistent with experimental measurements [10]. In the following, we will rely on the predictions produced by this validated

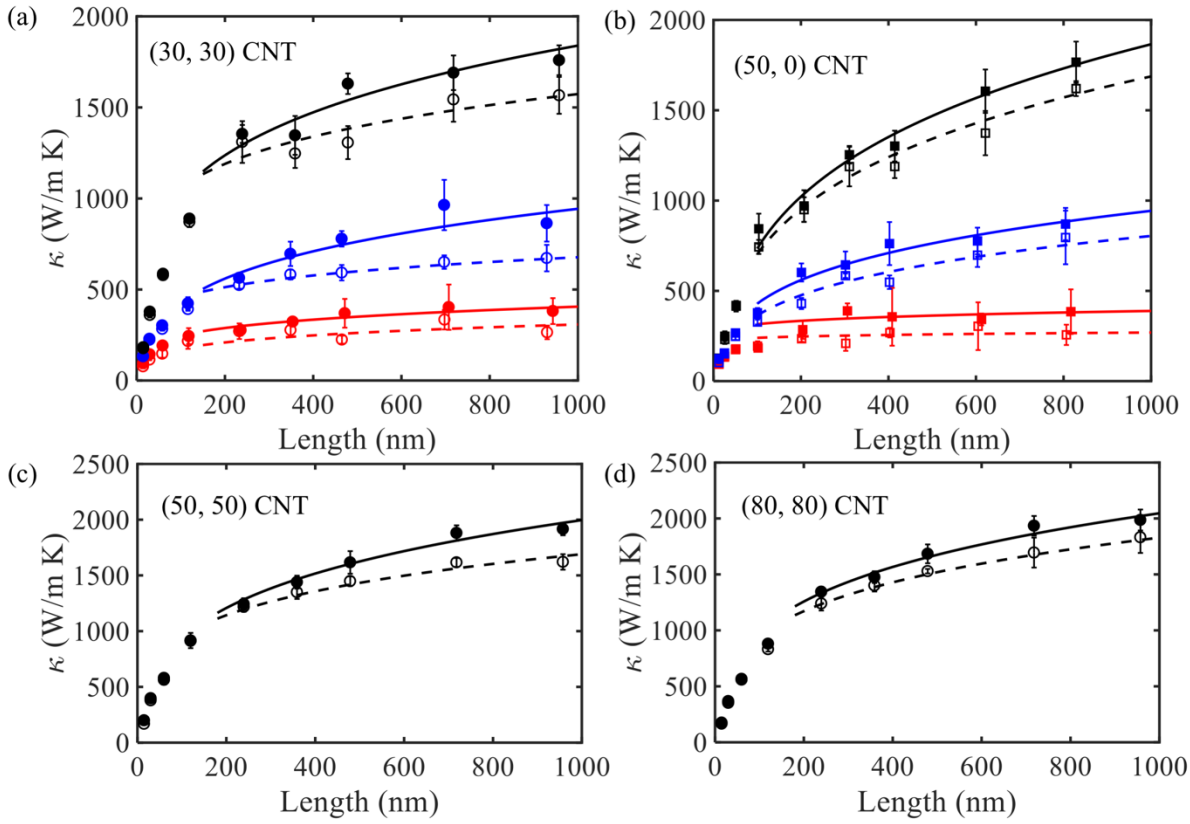

potential. Finally, we note that in Figure 4, the weak dependence of κ on CNT diameter and chirality is in agreement with previous literature [31].

Figure 4. κ of cylindrical (filled symbols) and collapsed (empty symbols,) (a) (30,30) CNTs (cross sectional area 4.39 $\mathrm{nm^2}$), (b) (50,0) CNTs (cross sectional area 4.23 $\mathrm{nm^2}$), (c) (50, 50) CNTs (cross sectional area 7.31 $\mathrm{nm^2}$) and (d) (80, 80) CNTs (cross sectional area 11.70 $\mathrm{nm^2}$) with different tube lengths, as calculated with re-optimized Tersoff (black), REBO (blue), and AIREBO (red) interatomic potentials. The regime in which κ extends from ballistic to diffusive is fitted as $\kappa \propto l^{0.2}$ for both cylindrical (solid line) and collapsed (dashed line) CNTs.

Figures 4a and 4b further reveal the impact on κ of the collapsed shape. In contrast with the behavior reported earlier in the bending-kink case [12], the ballistic transport is not affected by the formation of the nearly-circular edges. As transport evolves into the diffusive regime, a more significant κ reduction develops, meaning that the heat carrying phonons scatter more effectively than in the cylindrical case. In the re-optimized Tersoff potential description, we measured only an 11% κ reduction for the (30,30) collapsed CNTs at the largest length considered. The REBO and AIREBO potentials produce more substantial reductions, 22% and 31%, respectively, a trend that correlates with the diameter decrease of the nearly-circular edges described by these potentials, Figure 2. Figures 4c and 4d show a similar behavior in larger diameter armchair CNTs. Since the diameters of the nearly-circular edges are the same in the shown collapsed (50, 50) and (80, 80) CNTs (see Figure 2), the similar level of reduction in κ obtained in the wider collapsed CNTs suggest that the bi-layer vdW scattering is affecting κ to a lesser extent.

It is useful to recall that MD captures naturally anharmonic effects and various scattering mechanisms. Thus, the MD-computed κ reflects both phonon dispersion effects and the phonon relaxation times (τ_Z). A CNT presents four acoustic phonon branches: two radial-breathing transverse acoustic (ZA) (atomic movement perpendicular to the CNT axis), one twist (TA) (torsional movement around the axis), and one longitudinal (LA) branch (atomic movement along the axis). For large diameter cylindrical CNTs, the dispersion curves of these acoustic modes show very little deviation from the corresponding acoustic modes of graphene [31].

Phonon dispersion modifications could be expected when changes in the mechanical properties of a mono-layer occur [35]. However, the elastic properties of collapsed CNTs closely resemble those of their cylindrical counterparts. For example, MD simulations showed that

stretching and compressing cylindrical and collapsed CNTs leads to overlapping strain energy curves [15]. Corroborating this observation, here we find that the phonon dispersion and phonon density of states are affected in a minor fashion by the collapsed shape, Figures S3, S4 and S5 [30].

We have also performed a phonon spectral analysis [30, 36, 37] based on the MD trajectories in order to illustrate how the τ_Z of heat carrying modes are impacted by the cross-sectional collapse. In Table 1 we compare the calculated averaged lifetimes τ_Z of the ZA and TA phonon modes of a cylindrical and collapsed (80,80) CNTs at three selected wave vectors and frequency intervals. The reported values have a maximum of 11% uncertainty. It is noteworthy that the low-frequency ZA modes are especially important due to their significant contribution to the κ of larger diameter cylindrical CNTs [31]. When measured in the edge region of the collapsed CNT, we see that the τ_Z values of the ZA branch are reduced significant (up a factor of 3) at most frequency peaks. In contrast, the reduction of τ_Z in the bi-layer region is rather small. At the same time, the TA data (last column of Table 1) also indicates that τ_Z is negligibly impacted by the edge and bi-layer regions.

Table 1. Re-optimized Tersoff potential calculations. Comparison of τ_Z in cylindrical and collapsed (80,80) CNTs. The wave vector (units of $2\pi/a_z$, $a_z = 0.246$ nm). Each shown frequency ranges contain three phonon peaks. The lifetimes are listed in the order set by the magnitude of their frequency.

CNT Shape	**Wave vector ($2\pi/a_z$)**	**Freq. (THz)**	**τ_Z ZA (ps)**	**Freq. (THz)**	**τ_Z TA (ps)**
Cylindrical	0.48	2.9 – 4.4	50.0; 38.5; 41.7	12.8 – 16.0	23.8; 22.7; 22.8
	0.60	4.8 – 6.2	50.0; 62.5; 41.7	16.7 – 18.9	23.8; 20.8; 22.7

	0.72	6.4 – 8.4	55.6; 50.0; 62.5	19.2 – 22.6	27.8; 25.0; 31.2
Collapsed					
	0.48	2.9 – 4.4	41.7; 20.0; 16.7	12.8 – 16.0	23.8; 20.0; 22.7
Edges:	0.60	4.8 – 6.2	16.7; 35.7; 26.3	16.7 – 18.9	15.6; 20.8; 22.7
	0.72	6.4 – 8.4	25.0; 41.7; 33.3	19.2 – 22.6	20.0; 20.8; 22.7
	0.48	2.9 – 4.4	41.7; 38.5; 35.7	12.8 – 16.0	22.7; 20.0; 17.9
Bi-layer:	0.60	4.8 – 6.2	50.0; 55.6; 31.3	16.7 – 18.9	21.7; 20.8; 22.7
	0.72	6.4 – 8.4	55.6; 50.0; 55.6	19.2 – 22.6	25.0; 25.7; 27.8

In view of the minor changes in phonon dispersion, the above sampling of the lifetimes provides evidence that the small reduction in κ resulting from the cross sectional collapse is fostered by the double role played by the nearly-circular edges: (i) to increase in a gentle way the important ZA phonon scattering through the anharmonicity caused by the curvature strain [26] at the edges, and (ii) to "connect" the bi-layer region in a way that limits the cross-plane scattering typical of unconnected graphene layers. By limiting cross-plane scattering, the collapsed CNTs can maintain large phonon lifetimes for the in-plane conduction modes, especially for the low frequency ZA modes.

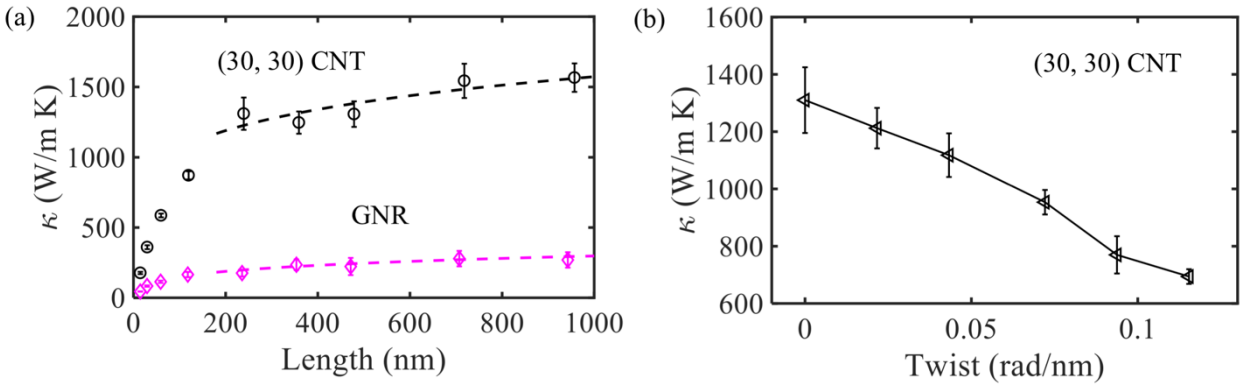

Figure 5. (a) Comparison of κ in collapsed (30,30) CNT and two-layer GNR with similar width

but rough edges. (b) κ vs. twist rate in a collapsed (30,30) CNT measuring 239.33 nm. Data is from the re-optimized Tersoff potential.

We further emphasize that the high κ of the collapsed CNTs is unusual given the fact that phonon propagation in atomically-thin graphene nanoribbons (GNRs) is especially sensitive to edge perturbation. As an example, Figure 5a compares the κ of collapsed (30,30) CNTs with that of bi-layer GNRs with similar widths but rough and open edges. (The rough open edges were created by opening the collapsed CNT and further eliminating atoms in a systematic manner while keeping the coordination number to at least two for the edge carbon atoms.) In contrast to the behavior of collapsed CNTs, the GNRs display diffusive phonon scattering and are not able to preserve the quasi-ballistic phononic transport. The longest GNR considered displays an approximately 83% reduction in κ. We note that the final κ=270 $W\ m^{-1}\ K^{-1}$ computed value is consistent with experimental measurements [17, 18].

Contrasting with the results obtained so far, Figure 5b shows that a gradually-applied twist deformation can reduce κ especially when the atomic-scale twist angle is very large. To explain this behavior, we ruled out potential changes in phonon scatterings of the nearly-circular or bilayer regions since the curvature at the edges and inter-layer separation do not change significantly with twist [16]. Instead, we recall that the twisted collapsed CNTs store shear strain [16]. We propose that the mechanism for enhancing phonon-phonon scattering is the anharmonicity in the inter-atomic potential created by the displacement of atoms from their equilibrium positions.

III. 2. Thermal Transport in Stacks of Collapsed CNTs

Collapsed CNTs are potentially attractive building blocks for forming mesoscale structures. Elliot et al. [14] investigated herringbone arrangements of collapsed CNT bundles

emerging under hydrostatic pressures. Inspired by the outcomes of recent experiments in stretching induced-alignment of CNT sheets [9], here we investigate tightly-packed architectures targeting ultra-high κ at the macro scale. The proposed packing, shown in Figure 1b for a system of collapsed (30,30) CNTs, accounts for the steric effect of stacking nearly-circular edges, which leads to a 49° incline of the periodicity vector in the perpendicular direction. The skewed stacking preserves the vdW contact between stacked bi-layer regions (vertical direction) and between the nearly-circular edges of CNTs in neighboring stacks (horizontal direction).

Using a simulation setup similar to that shown in Fig. 3, we computed κ along a skewed stack with different numbers of collapsed (30,30) CNTs. As can be seen from the results summarized in Figure 6b, κ becomes rapidly independent on the number of tubes, a behavior that resembles the weak layer-dependence of in-plane κ in few-layer graphene [20]. Notably, the converged κ shows only a 14% reduction from the isolated collapsed (30,30) CNT.

We have also evaluated the interfacial thermal resistance R between collapsed (30,30) CNTs. To verify our method, we have first computed R across two aligned cylindrical (30,30) CNTs at their equilibrium vdW distance. R across two (30, 30) cylindrical CNTs turned out to be $2.38\times10^{10}K/W$, a value that is significantly larger than the $9.69\times10^{9}K/W$ obtained in the collapsed case. The former value is in good agreement with what was obtained in previous studies [38, 39] and reflects the smaller number of carbon atoms in effective vdW contact. Note that in order to avoid defining the contact area between cylindrical CNTs, here we have

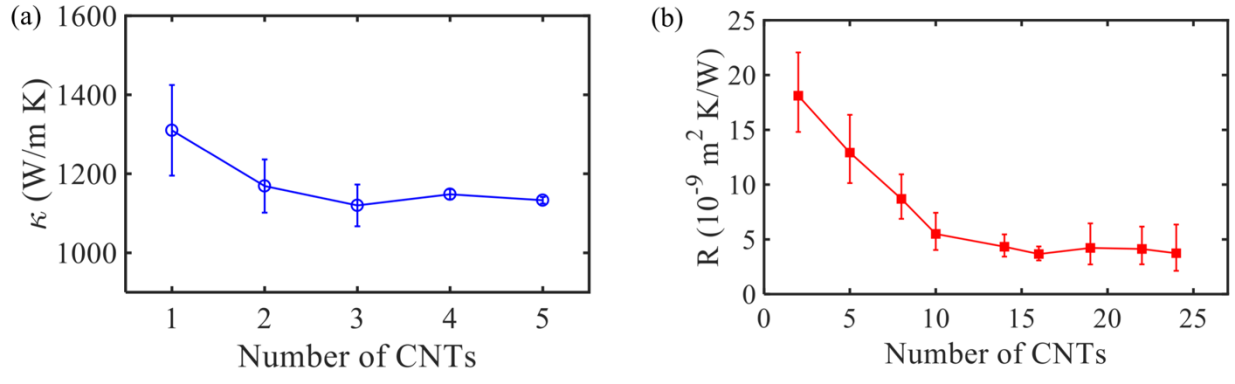

compared R in K/W units [38].

Figure 6. (a) κ of stacked-collapsed (30,30) CNTs. The length of each CNT is 239.33 nm. (c) R across the stacked collapsed (30,30) CNTs vs. the number of CNTs. The length of each CNT is 3.74 nm. Data is from the re-optimized Tersoff potential.

In spite of the good vdW contact, R between collapsed (30,30) CNTs is still large, a result that indicates that thermal transport in the stacked CNTs is strongly anisotropic. Figure 4b shows that R decreases with the increase in number of CNTs, and converges to 3.9×10^{-9} m^2 K/W, a value that is similar with R across few-layer graphene [40]. On the other hand, we expect that R between the nearly-circular edges of collapsed CNTs in neighboring stacks to be even larger, similar to R across small-diameter cylindrical CNTs [38, 39]

IV. CONCLUSION

The atomistic simulation results presented here indicate that collapsed CNTs and stacked-collapsed CNTs behave thermally like bi-layers and few-layer GNRs, respectively, but free from the diffusive phonon scattering associated with rough edges and cross-plane scattering. While κ of individual collapsed CNTs can be significantly reduced by torsional deformation, the stacked collapsed bundles should be more robust, as the torsional rigidity of few-layer graphene ribbons increases rapidly with the number of layers [41]. Our theoretical findings are especially important in the context of the recent progress in carbon composites. In general, κ of the CNT network measures only tens of W m^{-1} K^{-1}. This is because the network structure exhibits poor alignment and low packing densities, and R at the CNT-CNT junction is viewed as a main obstacle for effective thermal transport [3]. The proposed alignment of long CNTs into stacked collapsed architectures, experimentally achievable by stretching-induced alignment of the CNT sheet [9], presents potential for processing unidirectional thermal highways in lightweight

functional composite materials. The stacked architectures are further amenable to enhancing κ in the cross-plane direction by lowering the R between collapsed CNTs via polymer functionalization [42].

VI. AKNOWEDGEMENTS

This work was partially supported by an Early Stage Innovations grant from NASA's Space Technology Research Grants Program and by NSF CMMI 1332228. J. A.-G. greatly acknowledges support from the Albert Swanson Fellowship. T.D. thanks the Hanse Wissenschaftskolleg Delmenhorst for hospitality. Resources supporting this work were provided by the NASA High-End Computing Program through the NASA Advanced Supercomputing Division at Ames Research Center.

V. REFERENCES

[1] E.J. Siochi, J.S. Harrison, Structural nanocomposites for aerospace applications, MRS Bulletin **40**, 829 (2015).

[2] Q. Cheng, B. Wang, C. Zhang, Z. Liang, Functionalized carbon-nanotube sheet/bismaleimide nanocomposites: mechanical and electrical performance beyond carbon-fiber composites, Small **6**, 763 (2010).

[3] T. S. Gspann, S. M. Juckes, J. F. Niven, M. B. Johnson, J. A. Elliott, M. A. White, A. H. Windle, High thermal conductivities of carbon nanotube films and micro-fibres and their dependence on morphology, Carbon **114**, 160 (2017).

[4] S. Li, J. G. Park, Z. Liang, T. Siegrist, T. Liu, M. Zhang, Q. Cheng, B. Wang, C. Zhang, In situ characterization of structural changes and the fraction of aligned carbon nanotube networks produced by stretching, Carbon **50**, 3859 (2012).

[5] T. Dumitrică, M. Hua, B. I. Yakobson, Symmetry-, time-, and temperature-dependent strength of carbon nanotubes, Proc. Natl. Acad. Sci. USA **103**, 6105 (2006).

[6] E. Pop, D. Mann, Q. Wang, K. Goodson, H. Dai, Thermal conductance of an individual

single-wall carbon nanotube above room temperature, Nano Lett. **6**, 96 (2006).

[7] Q. Cheng, J. Bao, J.G. Park, Z. Liang, C. Zhang, B. Wang, High mechanical performance composite conductor: multi-walled carbon nanotube sheet/bismaleimide nanocomposites, Adv. Funct. Mat. **19**, 3219 (2009).

[8] R. Downes, S. Wang, D. Haldane, A. Moench, R. Liang, Strain-induced alignment Mechanisms of carbon nanotube networks, Adv. Eng. Mater. **17**, 349 (2015).

[9] R. D. Downes, A. Hao, J. G. Park, Y.-F. Su, R. Liang, B. D. Jensen, E. J. Siochi, K. E. Wise, Geometrically constrained self-assembly and crystal packing of flattened and aligned carbon nanotubes, Carbon **93**, 953 (2015).

[10] M. Fujii, X. Zhang, H. Xie, H. Ago, K. Takahashi, T. Ikuta, H. Abe, T. Shimizu, Measuring the thermal conductivity of a single carbon nanotube, Phys. Rev. Lett. **95**, 065502 (2005).

[11] J. Hone, M. Whitney, C. Piskoti, A. Zettl, Thermal conductivity of single-walled carbon nanotubes, Phy. Rev. B **59**, 2514 (1999).

[12] J. Ma, Y. Ni, S. Volz, T. Dumitrică, Thermal transport in single-walled carbon nanotubes under pure bending, Phys. Rev. Appl. 3, 024014 (2015); J. Ma, Y. Ni, T. Dumitrică, Thermal conductivity and phonon scattering in severely bent carbon nanotubes and bi-layer graphene, Mater. Today – Proc. 2, 3819 (2015).

[13] N. G. Chopra, L. X. Benedict, V. H. Crespi, M. L. Cohen, Fully collapsed carbon nanotubes, Nature **377**, 135 (1995).

[14] J. A. Elliott, J. K. W. Sandler, A. H. Windle, R. J. Young, M. S. P. Shaffer, Collapse of single-wall carbon nanotubes is diameter dependent, Phys. Rev. Lett. **92**, 095501 (2004).

[15] G. Gao, T. Çağin, W. A. Goddard III, Energetics, structure, mechanical and vibrational properties of single-walled carbon nanotubes, Nanotechnol. **9**, 184 (1998).

[16] D.-B. Zhang, T. Dumitrică, Effective strain in helical rippled carbon nanotubes: a unifying concept for understanding electromechanical response, ACS Nano 4, 6966 (2010). D.-B. Zhang, T. Dumitrică, Role of effective tensile strain in electromechanical response of helical graphene nanoribbons with open and closed armchair edges, Phys. Rev. B 85, 035445 (2012).

[17] M.-H. Bae, Z. Li, Z. Aksamija, P. N. Martin, F. Xiong, Z.-Y. Ong, I. Knezevic, E. Pop, Ballistic to diffusive crossover of heat flow in graphene ribbons, Nature Comm. **4**, 1734 (2013).

[18] A. V. Savin, Y. S. Kivshar, B. Hu, Suppression of thermal conductivity in graphene nanoribbons with rough edges, Phys. Rev. B **82**, 195422 (2010).

[19] S. Ghosh, W. Bao, D. L. Nika, S. Subrina, E. P. Pokatilov, C. N. Lau, A. A. Balandin, Dimensional crossover of thermal transport in few-layer graphene, Nature Mat. **9**, 555 (2010).

[20] W. R. Zhong, M. P. Zhang, B. Q. Ai, D. Q. Zheng, Chirality and thickness-dependent thermal conductivity of few-layer graphene: a molecular dynamics study, Appl. Phys. Lett. **98**, 113107 (2011).

[21] H. R. Barzegar, A. Yan, S. Coh, E. Gracia-Espino, C. Ojeda-Aristizabal, G. Dunn, M. L. Cohen, S. G. Louie, T. Wågberg, A. Zettl, Spontaneous twisting of a collapsed carbon nanotube, Nano Research **10**, 1942 (2017).

[22] S. Plimpton, Fast parallel algorithms for short-range molecular dynamics, J. Comput. Phys. **117**, 1 (1995).

[23] T. Dumitrică, R. D. James, Objective molecular dynamics J. Mech. Phys. Solids **55**, 2206 (2007).

[24] S. J. Stuart, A. B. Tutein, J. A. Harrison, A reactive potential for hydrocarbons with intermolecular interactions, J. Chem. Phys. **112**, 6472 (200).

[25] D. W. Brenner, O. A. Shenderova, J. A. Harrison, S. J. Stuart, B. Ni, S. B. Sinnott, A second-generation reactive empirical bond order (REBO) potential energy expression for hydrocarbons, J. Phys. Condens. Matter **14**, 783 (2002).

[26] I. Nikiforov, E. Dontsova, R. D. James, T. Dumitrică, Tight-binding theory of graphene bending, Phys. Rev. B **89**, 155437 (2014).

[27] J. Tersoff, Empirical interatomic potential for carbon, with applications to amorphous carbon, Phys. Rev. Lett. **61**, 2879 (1988).

[28] L. Lindsay, D. Broido, Optimized Tersoff and Brenner empirical potential parameters for lattice dynamics and phonon thermal transport in carbon nanotubes and graphene, Phys. Rev. B **81**, 205441 (2010).

[29] R. N. Salaway, L. V. Zhigilei, Molecular dynamics simulations of thermal conductivity of carbon nanotubes: Resolving the effects of computational parameters, Int. J. Heat Mass Transf. **70**, 954 (2014).

[30] See Supplemental Material at [URL will be inserted by publisher] for κ convergence test, collapsed tube stability under MD, computed phonon dispersion, phonon density of states, and for details on the calculations of the phonon relaxation times.

[31] A. Cao, J. Qu, Size dependent thermal conductivity of single-walled carbon nanotubes, J. Appl. Phys. **112**, 013503 (2012).

[32] J. R. Lukes, H. Zhong, Thermal conductivity of individual single-wall carbon nanotubes, J. Heat Transfer **129**, 705 (2007).

[33] N. Mingo, D.A. Broido, Carbon nanotube ballistic thermal conductance and its limits, Phy. Rev. Lett. **95**, 096105 (2005).

[34] J. Wang, J.-S. Wang, Carbon nanotube thermal transport: ballistic to diffusive, Appl. Phys. Lett. **88**, 111909 (2006).

[35] T. Zhu, E. Ertekin, Resolving anomalous strain effects on two-dimensional phonon flows: The cases of graphene, boron nitride, and planar superlattices, Phys. Rev. B **91**, 205429 (2015).

[36] T. Feng, B. Qiu, X. Ruan, Anharmonicity and necessity of phonon eigenvectors in the phonon normal mode analysis, J. Appl. Phys. **117**, 195102 (2015).

[37] J. A. Thomas, J. E. Turney, R. M. Iutzi, C. H. Amon, A. J. McGaughey, Predicting phonon dispersion relations and lifetimes from the spectral energy density, Phys. Rev. B **81**, 081411 (2010).

[38] C.-J. Hu, B.-Y. Cao, Thermal resistance between crossed carbon nanotubes: molecular dynamics simulations and analytical modeling, J. Appl. Phys. **114**, 224308 (2013).

[39] V. Varshney, S. S. Patnaik, A. K. Roy, B. L. Farmer, Modeling of thermal conductance at transverse CNT–CNT interfaces, J. Phys. Chem. C **114**, 16223 (2010).

[40] Y. Ni, Y. Chalopin, S. Volz, Significant thickness dependence of the thermal resistance between few-layer graphenes, Appl. Phys. Lett. **103**, 061906 (2013).

[41] E. Dontsova, T. Dumitrică, Nanomechanics of twisted mono- and few-layer graphene nanoribbons, J. Phys. Chem. Lett. **4**, 2010 (2013).

[42] Y. Ni, H. Han, S. Volz, T. Dumitrică, Nanoscale azide polymer functionalization: a robust solution for suppressing the carbon nanotube–polymer matrix thermal interface resistance, J. Phys. Chem. C **119**, 12193 (2015).